Supporting Information for:

High-temperature synthesis of small-sized Pt-Nb alloy catalysts on carbon supports for hydrothermal reactions

Shi-Long Xu, Shan-Cheng Shen, Wei Xiong, Shuai Zhao, Lu-Jie Zuo, Lei Wang, Wei-Jie Zeng, Sheng-Qi Chu, Ping Chen, Yue Lin, Kun Qian*, Weixin Huang, and Hai-Wei Liang*

* Corresponding author E-mail:

Hai-Wei Liang: hwliang@ustc.edu.cn; Kun Qian: qiankun@ustc.edu.cn

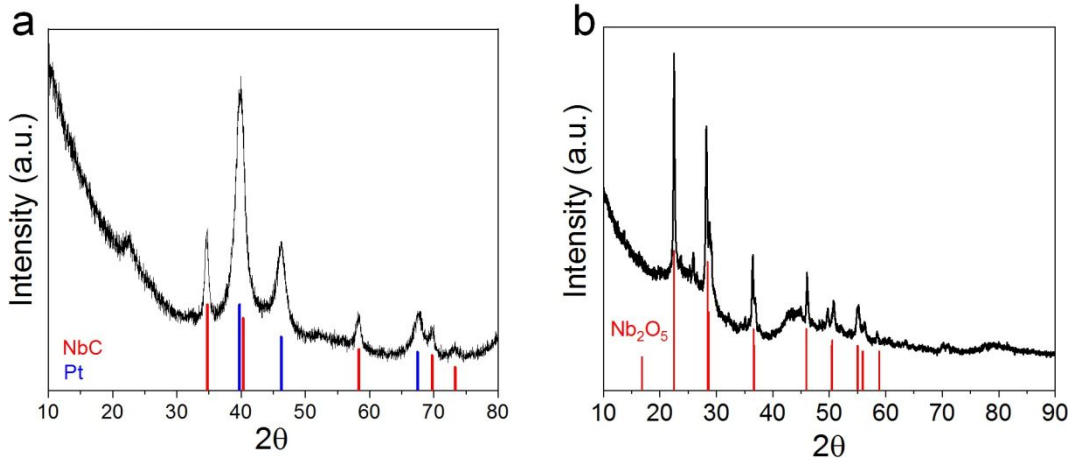

Figure S1. (a) PXRD patterns of Pt-Nb material synthesized by the wet-impregnation of H_2PtCl_6 and $NbCl_5$ onto BP2000 in an aqueous solution, indicating the mixture of niobium carbide and monometallic Pt. The standard peaks of Pt (JCDPDF no. 04-0802) and NbC (JCDPDF no. 38-1364) are shown in red and blue lines respectively for comparison. (b) PXRD patterns of monometallic Nb/BP2000 sample, indicating the presence of Nb_2O_5. The standard peaks of Nb_2O_5 (JCDPDF no. 27-1312) are shown in red lines for comparison.

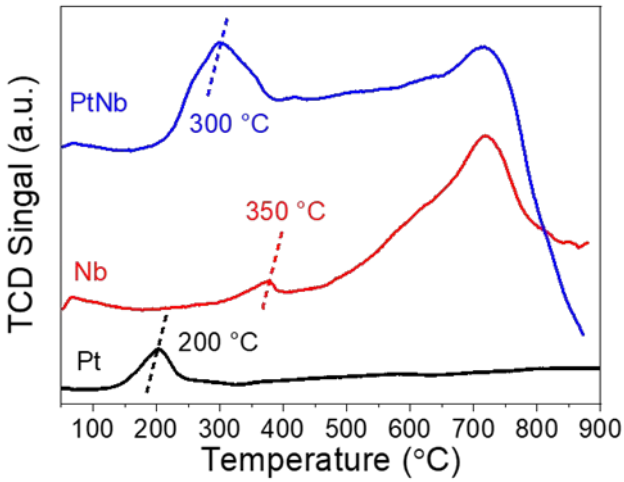

Figure S2. TPR profiles of the catalyst precursors. Although the monometallic Nb precursor was very difficult to reduce over carbon support, alloying Pt with Nb enabled us to observe the hydrogen spillover–assisted reduction of Nb species by Pt at 300 °C. The similar reduction peaks at around 720 °C in the Nb and Pt-Nb TPR profiles confirmed the presence of some isolated NbO_x in the PtNb alloy catalyst.

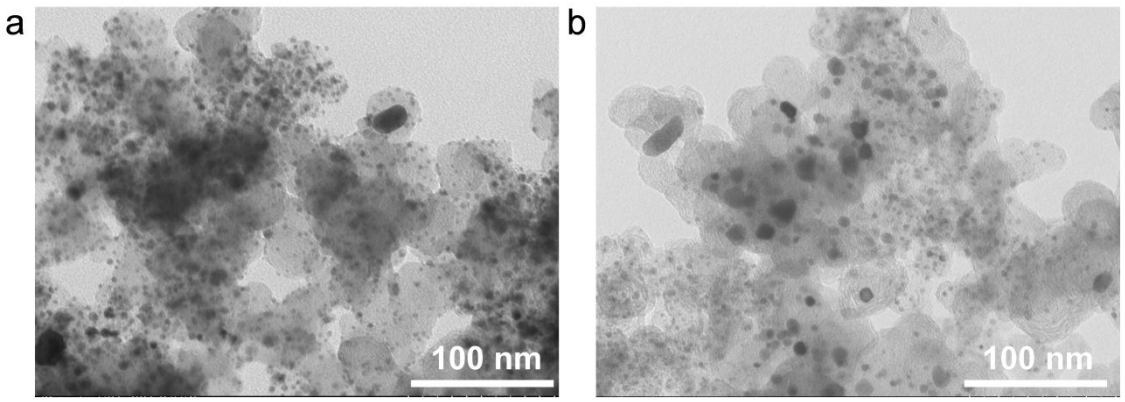

Figure S3. TEM images of the PtNb/Vulcan XC-72 (a) and PtNb/Kejen black EC-300JD (b).

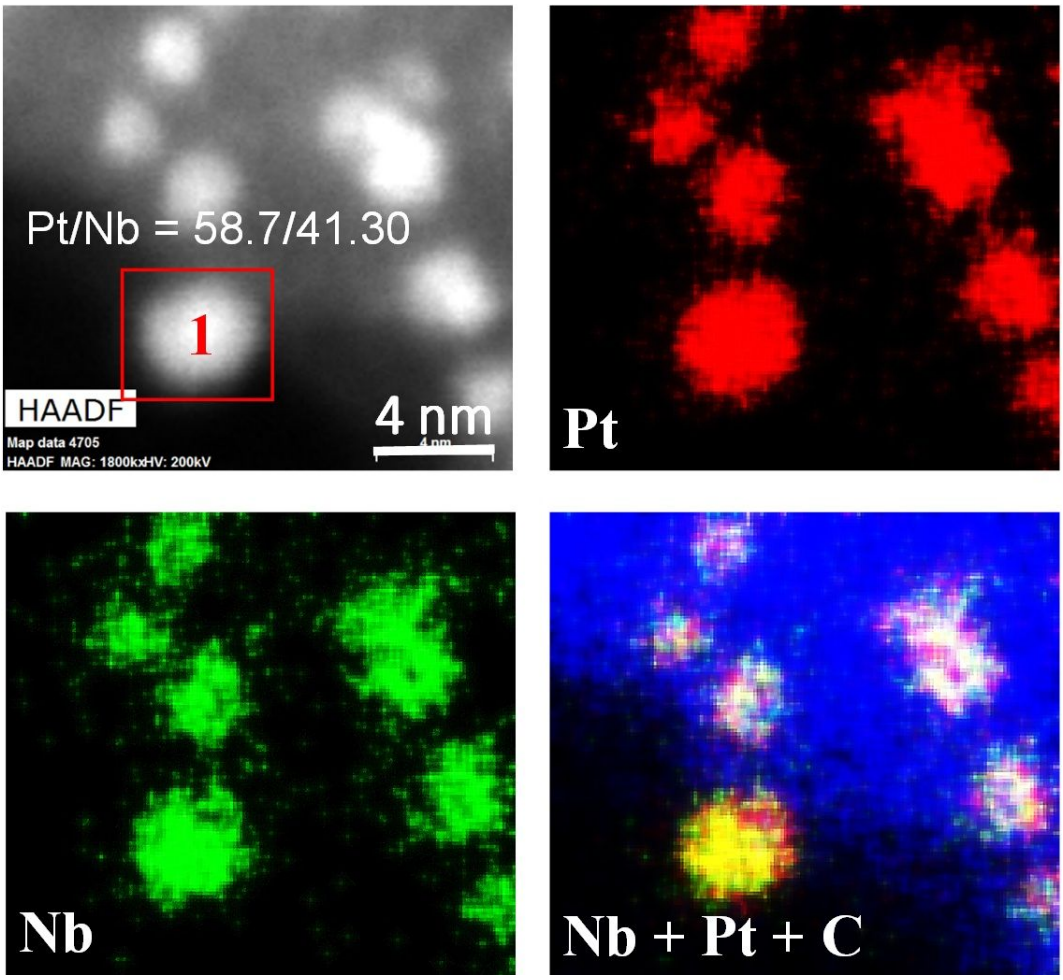

Figure S4. EDS elemental mapping of PtNb/BP2000, showing the well-alloyed Pt-Nb nanoparticles with the Pt/Nb atomic ratio close to the theoretical value of 1:1.

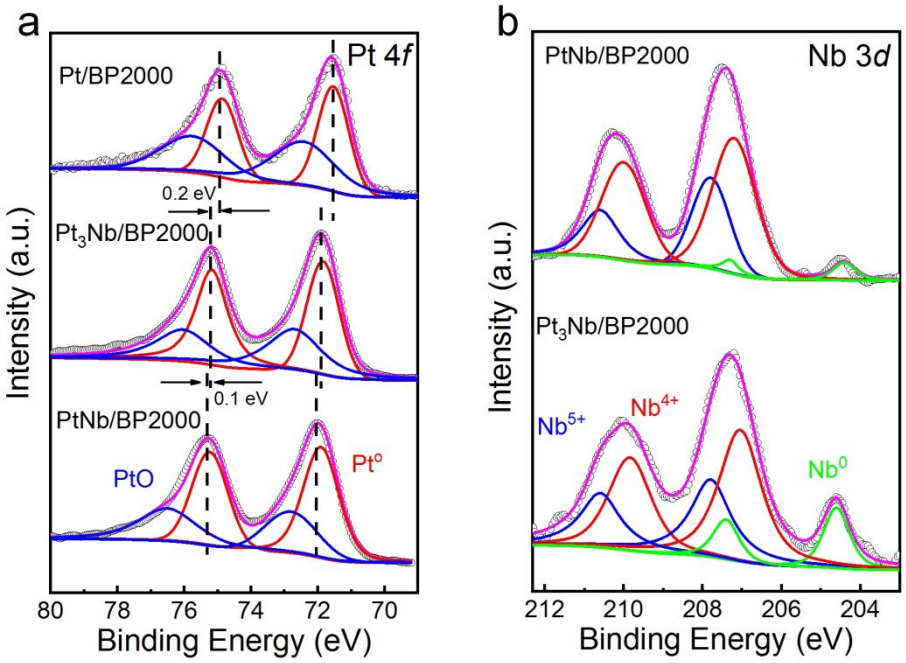

Figure S5. (a) Pt 4f region of XPS of Pt/BP2000, Pt_3Nb/BP2000, and PtNb/BP2000. (b) Nb 3d region of XPS of PtNb/BP2000 and Pt_3Nb/BP2000.

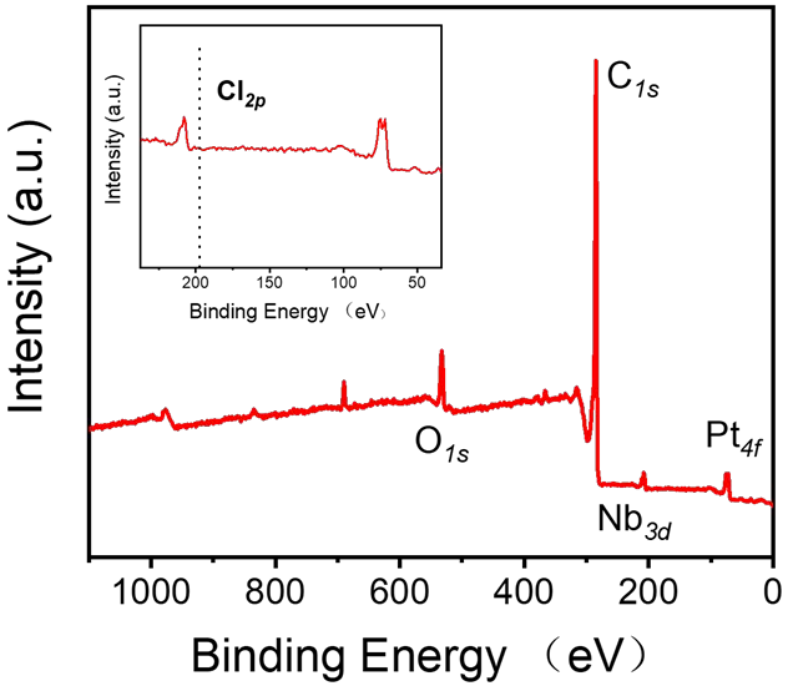

Figure S6. XPS survey of the PtNb/BP2000 catalyst.

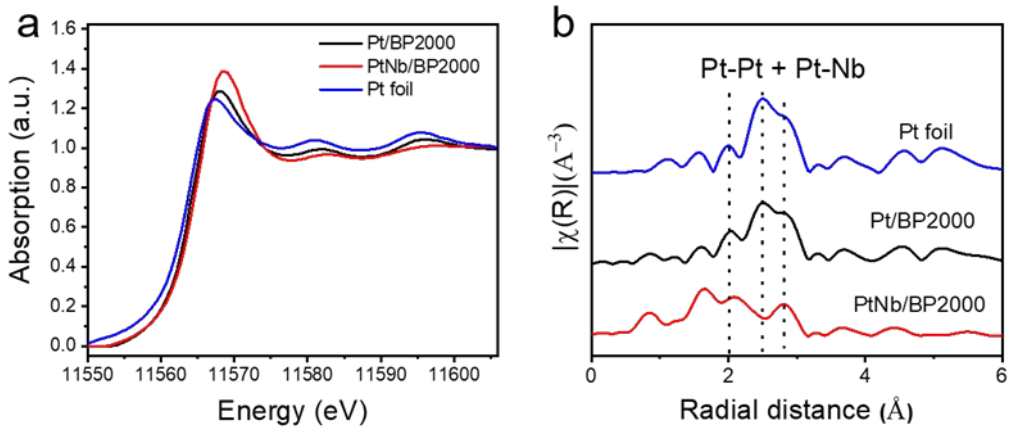

Figure S7. (a) XANES spectra and (b) Fourier transforms of EXAFS spectra at Pt L_3-edge of PtNb/BP2000 and reference catalysts (Pt/BP2000 and Pt foil).

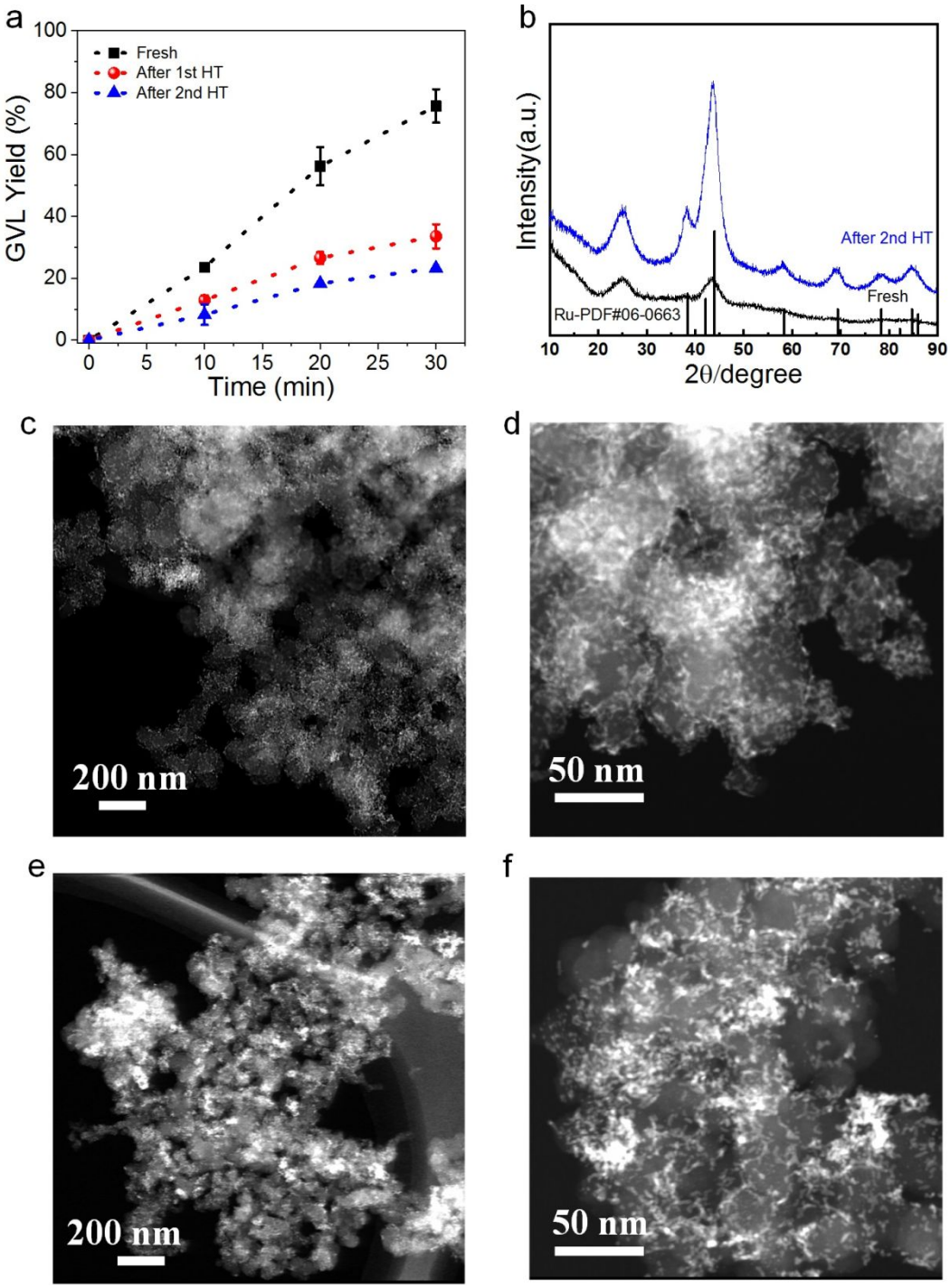

Figure S8. (a) Yield of GVL as a function of time for the Ru/C catalyst before and after two hydrothermal treatment runs. (b) PXRD pattern of Ru/C before and after two hydrothermal treatments. (c-f) HAADF images of the Ru/C catalyst before (c, d) and after (e, f) two hydrothermal treatment runs.

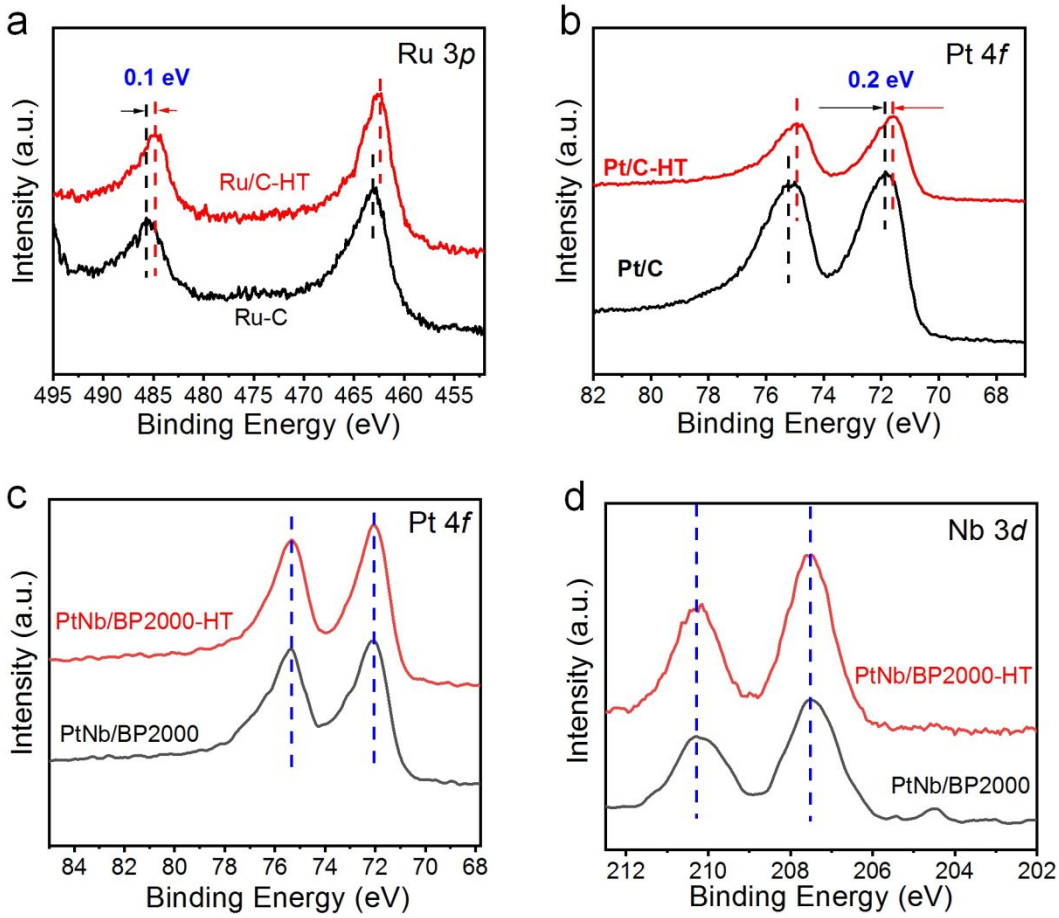

Figure S9. High resolution XPS spectra of fresh Ru/C, Pt/C, and PtNb/BP2000 catalysts and those after two hydrothermal treatment runs. (a) Ru 3p spectra of Ru/C. (b) Pt 4f spectra of Pt/C. (c-d) Pt 4f spectra (c) and Nb 3d (d) spectra of PtNb/BP2000.

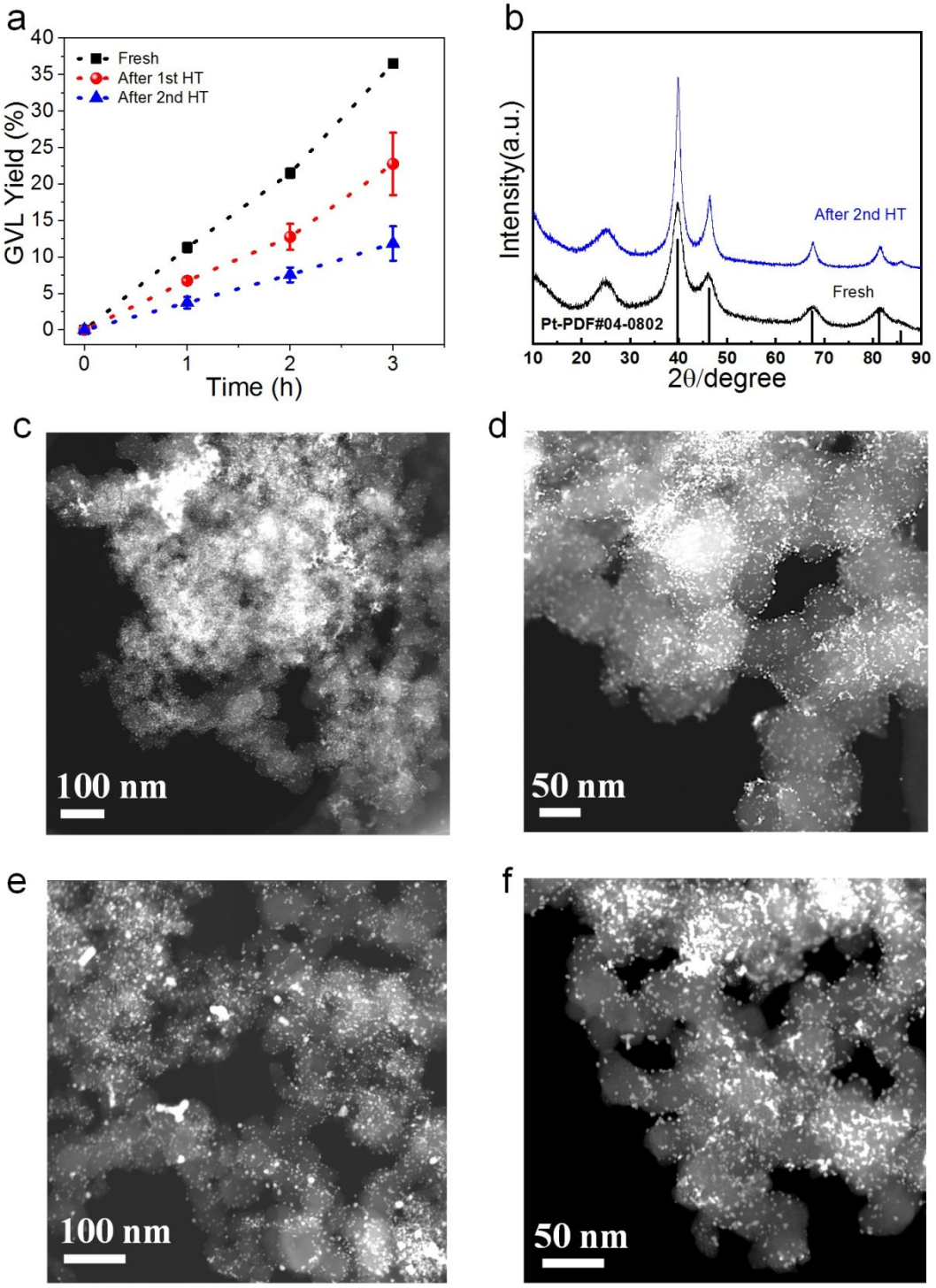

Figure S10. (a)Yield of GVL as a function of time for the Pt/C catalyst before and after two hydrothermal treatment runs. (b) PXRD pattern of the Pt/C catalyst before and after two hydrothermal treatment runs. (c-f) HAADF images of the Pt/C catalyst before (c, d) and after (e, f) two hydrothermal treatment runs.

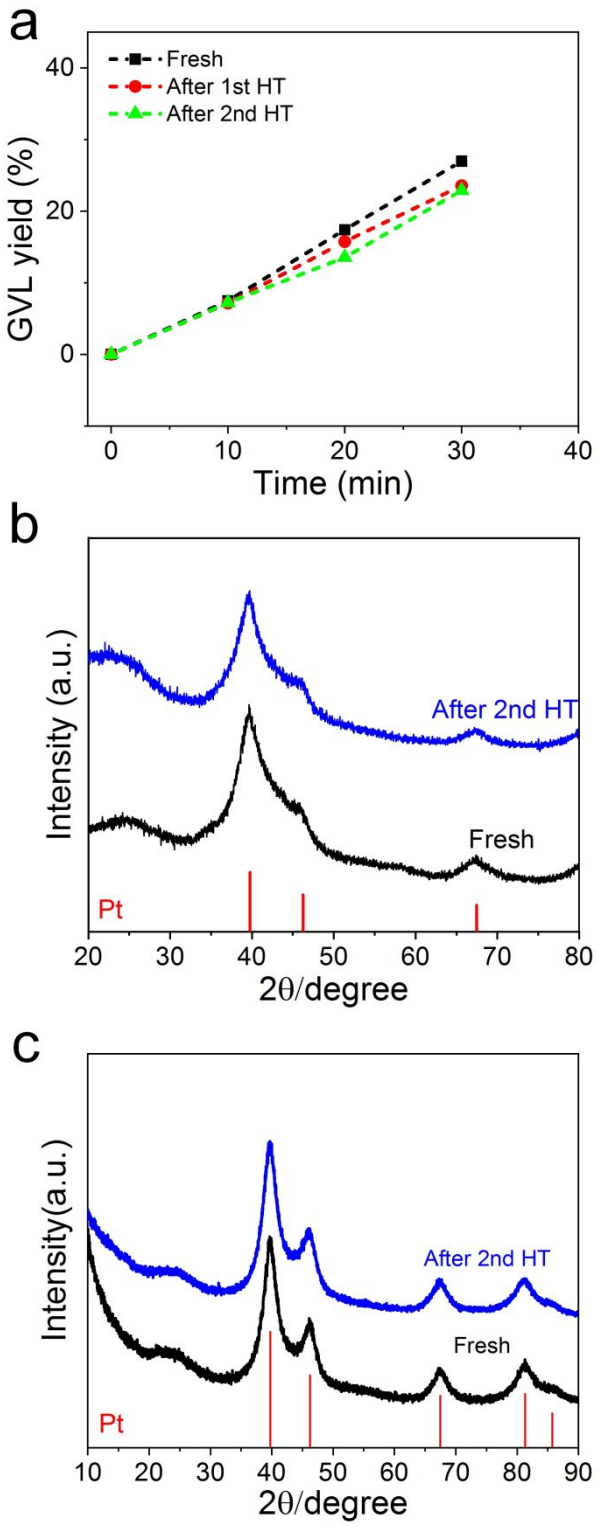

Figure S11. (a) PXRD pattern of PtNb/BP2000 before and after two hydrothermal treatment runs. (b)Yield of GVL as a function of time for the Pt_3Nb/BP2000 catalyst before and after two hydrothermal treatment runs. (c) PXRD pattern of the Pt_3Nb/BP2000 catalyst before and after two hydrothermal treatment runs.

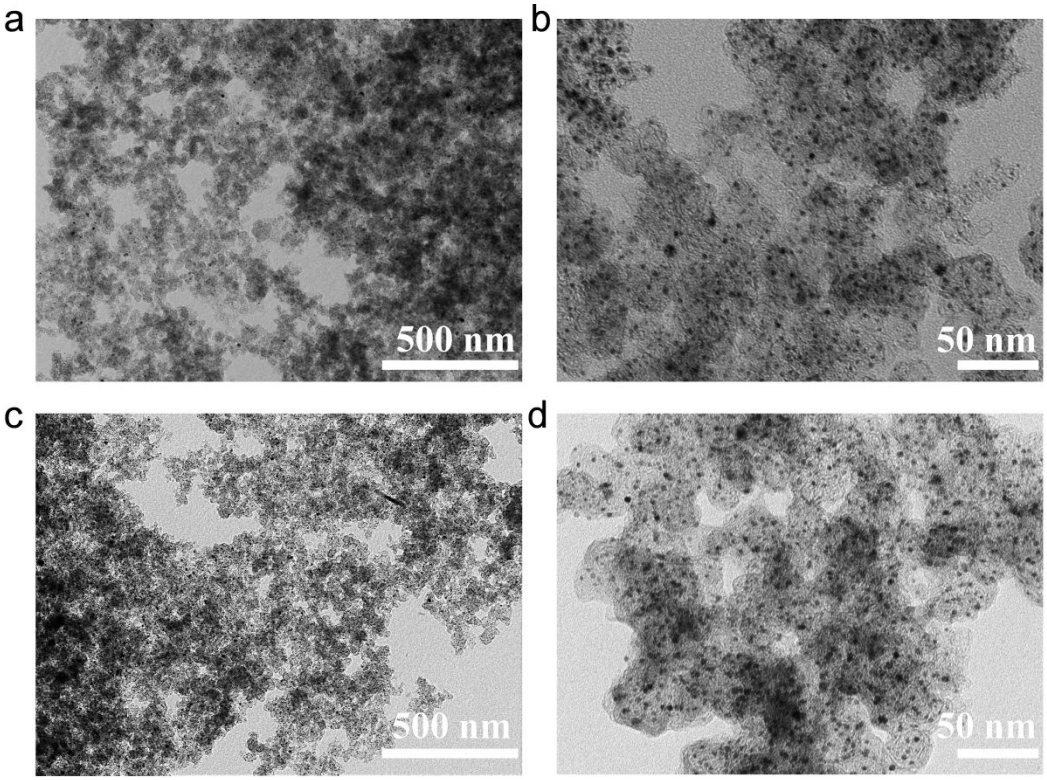

Figure S12. TEM images of the 20 wt% PtNb/BP2000 catalyst before (a, b) and after (c, d) WGS stability test.

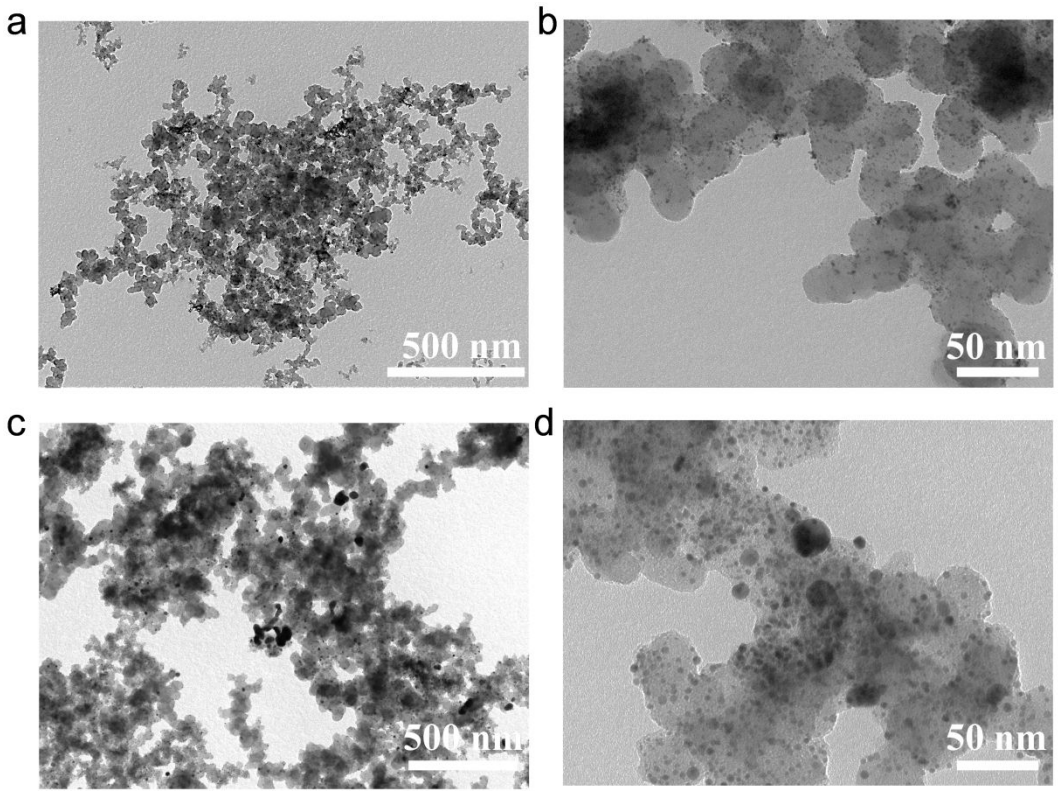

Figure S13. TEM images of the 20 wt% Pt/C catalyst before (a, b) and after (c, d) WGS stability test.

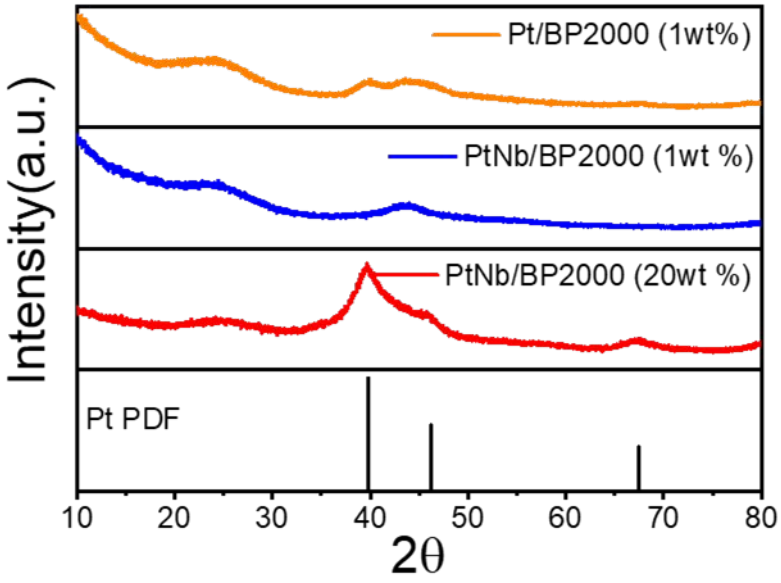

Figure S14. PXRD patterns of the PtNb/BP2000 (1 wt%) and PtNb/BP2000 (20 wt%) catalysts, clearly indicating the much smaller particle size for the low-loading catalyst.

Table S1. The compositional information of Pt_3Nb/BP2000 and PtNb/BP2000 based on the XPS analyses.

Sample	C (wt%)	O (wt%)	Pt (wt%)	Nb (wt%)	Pt/Nb
PtNb/BP2000	89.49	3.17	5.26	2.0	1.25
Pt_3Nb/BP2000	91.63	2.10	5.33	0.87	2.92

Table S2. Performance comparison of the Pt-Nb alloy catalysts with reported noble catalysts for the hydrogenation of LA to GVL.

Catalyst	TOF (s^{-1})	Reaction condition	Reference
PtNb/BP2000	**0.66**	**453K, 40 bar, in water**	**This work**
Pt_3Nb/BP2000	**0.49**	**453K, 40 bar, in water**	**This work**
AuPd/TiO_2	0.102	473 K, 40 bar, in dioxane	1
RuPd/TiO_2	0.638	473 K, 40 bar, in dioxane	1
Ru/TiO_2	0.239	473 K, 40 bar, neat LA	2
Ru/C	0.293	463 K, 12 bar, neat LA	3
Ru/C	0.033	403 K, 12 bar, ethanol/ water	3
Ru/TiO_2	0.027	403 K, 12 bar, ethanol/ water	3
Ru/TiO_2	0.0059	423 K, 35 bar, in water	4
Ru/TiO_2	0.0137	423 K, 35 bar, in water	4
Pd/C	0.002	538 K, 1 bar, in dioxane	5
Ru/C/Amberlyst-70	0.155	343 K, 30 bar, in water	6
RuSn/C	0.008	493 K, LA and FA in alkyl-phenolsolvent	7
RuRe/C	0.00049	423 K, 5 bar, equimolar LA and FA, and H_2SO_4 (0.5 mol/L)	8
Au/ZrO_2	0.189	423 K, 5 bar, equimolar LA and FA	9
RuNi/C	0.606	423 K, 45 bar, LA in water	10
Ir@ZrO_2@C	0.034	453K, 40bar, LA in water	11
Ru/MIL-101(Cr)	0.020	343K, 10 bar, LA in water	12
$Ru_{1.5}$@TNph-PTA	2.45	423K, 10 bar, LA in water	13

Table S3. The amount of metal leaching into the liquid phase after the hydrothermal treatments as determined by ICP-MS.

Sample	Metal leaching (%)	
	Pt	Ru
Pt_3Nb/BP2000	0.03*/0.05#	–
PtNb/BP2000	0.05*/0.09#	–
Pt/C	0.12*/0.13#	–
Ru/C	–	4.27*/10.10#

* The amount of metal leaching after the 1st hydrothermal treatment.

The amount of metal leaching after the 2nd hydrothermal treatment.

REFERENCES

(1) Luo, W.; Sankar, M.; Andrew, M. B.; He, Q.; Christopher, J. K.; Pieter, C. B.; Weckhuysen, B. M. High performing and stable supported nano-alloys for the catalytic hydrogenation of levulinic acid to γ-valerolactone. *Nat. Commun.* **2015**, 6, 6540.

(2) Luo, W.; Deka, U.; Beale, A. M.; van Eck, E. R.; Bruijnincx, P. C.; Weckhuysen, B. M. Ruthenium-catalyzed hydrogenation of levulinic acid: Influence of the support and solvent on catalyst selectivity and stability. *J. Catal.* **2013**, 301, 175-186.

(3) Shaal, M. G.; Wright, W. R.; Palkovits, R. Exploring the ruthenium catalysed synthesis of γ-valerolactone in alcohols and utilisation of mild solvent-free reaction conditions. *Green Chem.* **2012**, 14, 1260-1263.

(4) Goyal, R.; Sarkar, B.; Bag, A.; Siddiqui, N.; Dumbre, D.; Lucas, N.; Bhargava, S. K.; Bordoloi, A. Studies of synergy between metal-support interfaces and selective hydrogenation of HMF to DMF in water. *J. Catal.* **2016**, 340, 248-260.

(5) Upare, P. P.; Lee, J.-M.; Hwang, D. W.; Halligudi, S. B.; Hwang, Y. K.; Chang, J.-S. Selective hydrogenation of levulinic acid to γ-valerolactone over carbon-supported noble metal catalysts. *J. Ind. Eng. Chem.* **2011**, 17, 287-292.

(6) Galletti, A. M. R.; Antonetti, C.; De Luise, V.; Martinelli, M. J. G. C. A sustainable process for the production of γ-valerolactone by hydrogenation of biomass-derived levulinic acid. *Green Chem.* **2012**, 14, 688-694.

(7) Alonso, D. M.; Wettstein, S. G.; Bond, J. Q.; Root, T. W.; Dumesic, J. A. Production of biofuels from cellulose and corn stover using alkylphenol solvents. *ChemSusChem* **2011**, 4, 1078-1081.

(8) Braden, D. J.; Henao, C. A.; Heltzel, J.; Maravelias, C. C.; Dumesic, J. A. Production of liquid hydrocarbon fuels by catalytic conversion of biomass-derived levulinic acid. *Green Chem.* **2011**, 13, 1755-1765.

(9) Du, X. L.; He, L.; Zhao, S.; Liu, Y. M.; Cao, Y.; He, H. Y.; Fan, K. N. Berichtigung: Hydrogen-Independent Reductive Transformation of Carbohydrate Biomass into γ-Valerolactone and Pyrrolidone Derivatives with Supported Gold Catalysts. *Angew. Chem. Int. Ed.* **2011**, 123, 7961-7965.

(10) Yang, Y.; Gao, G.; Zhang, X.; Li, F. Facile fabrication of composition-tuned Ru–Ni bimetallics in ordered mesoporous carbon for levulinic acid hydrogenation. *ACS Catal.* **2014**, 4, 1419-1425.

(11) Cao, W.; Lin, L.; Qi, H.; He, Q.; Wu, Z.; Wang, A.; Luo, W.; Zhang, T. In-situ synthesis of single-atom Ir by utilizing metal-organic frameworks: An acid-resistant catalyst for hydrogenation of levulinic acid to γ-valerolactone. *J. Catal.* **2019**, 373, 161-172.

(12) Guo, Y.; Li, Y.; Chen, J.; Chen, L. Hydrogenation of levulinic acid into γ-valerolactone over ruthenium catalysts supported on metal–organic frameworks in aqueous medium. *Catal. Let.* **2016**, 146, 2041-2052.

(13) Wang, Q.; Ling, X.; Ye, T.; Zhou, Y.; Wang, J. Ionic mesoporous polyamides enable highly dispersed ultrafine Ru nanoparticles: a synergistic stabilization effect and remarkable efficiency in levulinic acid conversion into γ-valerolactone. *J. Mater. Chem. A* **2019**, 7, 19140-19151.